Spatial sharpening of Thematic Mapper data using a multiband approach

Victor T. Tom
Mark J. Carlotto
Daniel K. Scholten
The Analytic Sciences Corporation
One Jacob Way
Reading, Massachusetts 01867

Abstract. A new image enhancement technique has been applied to enhance Landsat-4 Thematic Mapper (TM) thermal infrared (IR) imagery and has improved its effective ground resolution from 120 m to 30 m. The technique is based on an adaptive multiband least squares (LS) method for computing an optimal image estimate from reference images, and a frequency domain replacement step. The approach relies on the assumption that at a sufficiently small resolution registered TM imagery data are locally correlated across the bands. Using the local correlation property, visible and IR reference bands are used to predict the thermal IR image data. The prediction estimate is then used to augment the spatial high frequency information in the original thermal data. Preliminary experiments enhancing 120 m IR imagery (simulated degradation) to 30 m resolution show a signal-to-noise ratio improvement of 19 dB.

Subject terms: image processing; digital image processing; image enhancement; spatial enhancement; adaptive least squares; multiband linear prediction; Landsat-4; Thematic Mapper; thermal imagery.

Optical Engineering 24(6), 1026-1029 (November/December 1985).

CONTENTS

1. INTRODUCTION

Spatial enhancement of imagery is normally accomplished by amplifying the magnitude of the high spatial frequency portion of the spectrum. This type of approach is normally limited to the portion of the spectrum where a high signal-to-noise ratio exists, and consequently only modest gains in resolution can be achieved. Super-resolution techniques attempt to improve the resolution by spectral extrapolation using other a priori information such as positivity or finite extent.[1] These techniques yield poor results for general imagery, however, because the phase estimation in the extrapolated spectrum is typically noisy. The one factor that all these enhancement algorithms have in common is that they do not utilize information other than from the image itself. For the specific problem of enhancing TM thermal data, a *multiband* approach offers the ability to integrate high spatial frequency information from the visible and infrared (IR) bands into the thermal data. The thermal band enhancement technique is based on an adaptive multiband least squares (LS) method for estimating the thermal data and, secondly, a frequency replacement step for constraining the enhanced thermal data to be consistent with the original data.

The organization of the remaining sections is as follows. Section 2 reviews the Thematic Mapper sensors and characteristics of the imagery data relevant to the enhancement procedure. Section 3 discusses the main assumption of this paper: the local correlation property of multispectral imagery data. A detailed description of the enhancement algorithm, covering the LS and the frequency replacement procedures, is presented in Sec. 4, followed by a discussion concerning window size and number of reference bands in Sec. 5. Section 6 presents examples of the performance of the enhancement procedure on simulated IR and real thermal IR data at 120 m resolution. The last section summarizes and suggests other applications for the adaptive LS technique.

2. LANDSAT THEMATIC MAPPER DATA

The Thematic Mapper is one of several types of instruments carried aboard the Landsat-4 satellite. The TM collects data in seven spectral bands (visible and IR wavelengths), which are summarized in Table I. The spatial resolution of the TM is 30 m, except for the thermal IR band, which is 120 m. The ground-processed thermal IR data are interpolated by factors of four in each direction to make the data sets consistent in size. Since the goal is to use correlated spatial information from the visible and reflective IR bands to enhance the emissive thermal band, the image bands have to be accurately registered. Based on Thematic Mapper images analyzed so far, the band-to-band registration is very good except for the thermal band.[2] For the Kansas scene in this paper, the thermal band required a shift of four pixels in the x and two in the y direction in order to align it with the visible bands. Minor shifts (less than one pixel) were also applied to the other bands.

3. CORRELATION OF TM DATA

For certain agricultural scenes, Thematic Mapper data exhibit a high degree of interband correlation.[3] TM bands 1, 2, and 3 have a high positive correlation due to the nature of ground cover conditions, such as bare soil and vegetation. Band 7 (mid-IR) has a strong

Paper 2057 received Aug. 17, 1984; revised manuscript received March 6, 1985; accepted for publication March 25, 1985; received by Managing Editor April 15, 1985. This paper is a revision of Paper 504-51 which was presented at the SPIE conference on Applications of Digital Image Processing VII, Aug. 21-24, 1984, San Diego, Calif. The paper presented there appears (unrefereed) in SPIE Proceedings Vol. 504.

TABLE I. Landsat Thematic Mapper Spectral Bands

Band number	Wavelength (μm)	Region
1	0.45–0.52	visible
2	0.52–0.60	visible
3	0.63–0.69	visible
4	0.76–0.90	near-IR
5	1.55–1.75	middle-IR
7	2.08–2.35	middle-IR
6	10.4–12.5	thermal IR

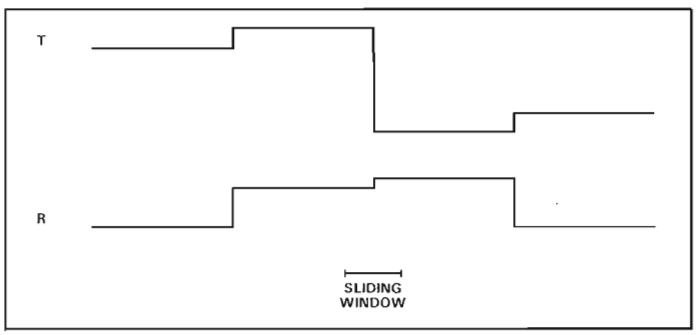

Fig. 1. 1-D cross sections of simulated thermal and IR data.

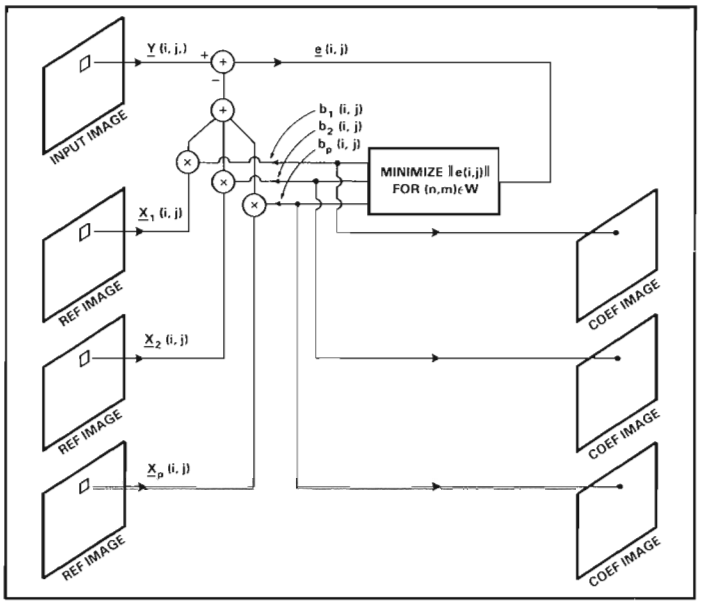

Fig. 2. 2-D adaptive multiband LS structure.

correlation with bands 1, 2, 3, and 5, and band 4 is relatively independent of the visible bands. The thermal IR band 6 is relatively independent of all the other bands. The degree of overall correlation is not only subject to the type of scene but also the time of year the imagery is acquired.

Edge information, however, appears highly correlated across all the different bands of TM data, independent of scene and time of year.[4] This suggests that TM bands are also *locally* correlated. Consider the following simplified example: Let T and R represent one-dimensional cross sections of thermal and IR data, respectively (both at 120 m resolution). As illustrated in Fig. 1, the signals overall have a low correlation factor. The edge locations are almost identical, however, yielding high correlations when the analysis window is small compared to the signal variations (see Fig. 1). Notice that the correlation is approximately one for the relatively constant regions. When the window overlaps an individual edge, the correlation is approximately one or minus one. Recently, local 1-D correlation was exploited to interpolate across the individual line dropouts using adjacent TM bands.[5]

Local correlation becomes more complicated for the 2-D case. Because of the additional degree of freedom, high local correlations are less likely at multiple region boundaries. In this case, a linear combination of reference bands may be necessary to construct a reference that is locally correlated everywhere with the image of interest.

4. ENHANCEMENT APPROACH

Exploiting the assertion that multiband images are correlated locally, one can use visible and reflective IR images to enhance the thermal IR image. The adaptive multiband enhancement procedure entails several steps:

(1) Filter bands 1 through 5 and band 7 to 120 m resolution.
(2) Use adaptive LS method to generate prediction coefficients (PC) for band 6.
(3) Generate optimal estimate for band 6 using PCs and bands 1 through 5 and band 7 at 30 m resolution.
(4) High-pass filter band 6 estimate and combine with original data for band 6.

In order to reduce computation time, the LS method can be performed on the subsampled reduced resolution images, thus reducing the computational burden by a factor of 16. The PC images are then interpolated (by 4 in x and y) prior to generating the optimal estimation for band 6. The two key processing steps, adaptive LS predictor and frequency replacement, are described in greater detail in the following sections.

4.1. Adaptive LS multiband predictor

Using a linear prediction approach, the thermal image estimate is formed by a weighted linear combination of reference images in which the weights change adaptively over the entire image. This construct is analogous to adaptive LS filters for 1-D signals and is illustrated in Fig. 2. A synchronized 2-D window slides over the degraded image (to be estimated) and the reference images. The output of the windows can be treated as vectors of data. The coefficients b_i form the estimate $\hat{y}$ (for the center pixel of the window) while being continually adjusted to minimize the error vector **e**. For a given location of the sliding prediction window, one can represent the (to be estimated) image **y** as

$$\begin{bmatrix} y_1 \\ y_2 \\ \cdot \\ \cdot \\ y_w \end{bmatrix} = \begin{bmatrix} 1 & x_{11} & x_{12} & \cdots & x_{1p} \\ 1 & x_{21} & x_{22} & \cdots & x_{2p} \\ \cdot & \cdot & \cdot & \cdots & \cdot \\ \cdot & \cdot & \cdot & \cdots & \cdot \\ 1 & x_{w1} & x_{w2} & \cdots & x_{wp} \end{bmatrix} \begin{bmatrix} b_0 \\ b_1 \\ \cdot \\ \cdot \\ b_p \end{bmatrix} + \begin{bmatrix} e_1 \\ e_2 \\ \cdot \\ \cdot \\ e_w \end{bmatrix} \quad (1)$$

The number of reference images is equal to p, the number of data values within each window is equal to w, and $w > p$. In practice, $w > p+1$ so that Eq. (1) is overdetermined. Alternatively, Eq. (1) can be written in vector matrix form as

$$\mathbf{y} = \mathbf{X}\mathbf{b} + \mathbf{e} , \quad (2)$$

where the matrix **X** contains the concatenated vectors of reference data as well as a constant vector. One can also write Eq. (2) as

$$\mathbf{y} = \hat{\mathbf{y}} + \mathbf{e} , \quad (3)$$

where $\hat{\mathbf{y}}$ is the optimal estimate for **y**.

The LS solution for the predictor $\hat{\mathbf{y}}$ is computed by solving for the set of coefficients **b** that minimize the following error norm:

$$\|\mathbf{e}\|^2 = (\mathbf{y} - \mathbf{X}\mathbf{b})^T (\mathbf{y} - \mathbf{X}\mathbf{b}) \ . \quad (4)$$

Minimizing the quantity in Eq. (4) is equivalent to solving the set of normal equations

$$(\mathbf{X}^T\mathbf{X})\mathbf{b} = \mathbf{X}^T\mathbf{y} \quad (5)$$

for the coefficient vector **b**. In 1-D signal linear prediction, Eq. (5) can be efficiently solved using a recursive approach. Since the 1-D window update involves adding and subtracting only one data value, the matrix $\mathbf{X}^T\mathbf{X}$ can be updated by shifting and adding one column and row of data. For the 2-D case, however, the 2-D window update involves adding an entire column of new image data. Therefore, the updating procedure for the matrix $\mathbf{X}^T\mathbf{X}$ for the 2-D window becomes more complicated. It so happens that the order of complexity for the 2-D update is the same as for the direct solution of Eq. (5).[6] As a consequence, our implementation of the 2-D linear prediction involved the straightforward solution; i.e.,

$$\mathbf{b} = (\mathbf{X}^T\mathbf{X})^{-1} (\mathbf{X}^T\mathbf{y}) \ . \quad (6)$$

The execution of this procedure yields an optimal estimate $\hat{\mathbf{y}}(n,m)$ and a set of prediction coefficients $\mathbf{b}(n,m)$, which have been computed adaptively over the domain of the 2-D sliding window.

In order to avoid erroneous solutions resulting from an ill-conditioned matrix $(\mathbf{X}^T\mathbf{X})$, a twofold approach was implemented. First, Eq. (6) is efficiently calculated, line by line, in an array processor. A second procedure is invoked to update the solution whenever $\mathbf{X}^T\mathbf{X}$ becomes ill-conditioned. This second procedure solves Eq. (1) by permuting the columns of **X** such that **X** is partitioned as $\mathbf{X} = (\mathbf{X1}, \mathbf{X2})$, where **X1** is w by p1 and has rank p1. It then solves for the least squares solution, setting to zero the elements of **b** that correspond to **X2**.

4.2. Spatial frequency replacement

The frequency replacement step is basically a nonlinear procedure to combine data in the spatial frequency domain. For a given spatial frequency range, the replacement algorithm allows one to replace the phase or magnitude (or both) of a signal with the phase and/or magnitude of the computed optimal estimate of the signal. In order to enhance the spatial resolution of data, the replacement procedure reduces to low-pass filtering the degraded data, high-pass filtering the optimal estimator, and adding the filtered results (in the Fourier domain); i.e.,

$$\tilde{Y}(k,l) = H_{lp}Y(k,l) + H_{hp}\hat{Y}(k,l) \ , \quad (7)$$

where the cutoff frequency of H_{lp} is chosen as low as possible such that

$$Y(k,l) = H_{lp}Y(k,l) \ . \quad (8)$$

The high-pass filter is the complementary filter given by

$$H_{hp}(k,l) = 1 - H_{lp}(k,l) \ . \quad (9)$$

One interpretation of Eq. (7) is that the low spatial frequency information is preserved (the truth data are not distorted) and it is supplemented with high frequency information from some reference. An alternative, and simpler, enhancement can be derived simply by using a different image band to high-pass filter, i.e., using TM band 5 to augment a degraded TM band 6. This simpler method is compared to the full method in the examples section.

5. WINDOW SIZE AND REFERENCE BANDS CONSIDERATIONS

An error analysis was then computed for the estimation of TM band 7 by the other bands using various window sizes and numbers of reference bands at full resolution. The imagery chosen was an agricultural area in Kansas (8-bit imagery). A gray-level rms error [$\|\mathbf{e}\|$ in Eq. (4)] was calculated for each window location and then averaged over all locations. These rms error figures are tabulated in Table II. From this table one observes that the error decreases rapidly with decreasing window size. Secondly, increasing the number of reference bands will also decrease the estimation error.

TABLE II. Average Gray-Level rms Error

No. of bands	Window size				
	63×63	31×31	15×15	7×7	3×3
1	17.58	14.36	12.03	8.25	4.43
2	17.29	13.97	11.74	7.83	3.71
4	12.51	9.98	8.35	5.55	2.08
6	10.32	7.89	6.44	4.37	1.14

TABLE III. Mean Square Gray-Level Error Residuals

Unenhanced	Simple filter	LS method
19.06	8.51	2.21

6. IMAGERY EXAMPLES

An initial version of the adaptive LS technique was implemented using a minicomputer and an array processor. The processed examples in this section include spatially sharpening Landsat TM middle-IR and thermal IR imagery.

As a test of the procedure, we first degrade a TM middle-IR image (band 7) from 30 m to 120 m resolution and then restore it to 30 m resolution. The purpose of degrading an IR band is so that we can compare the enhanced image with a known original. An original TM band 7 image is presented in Fig. 3. Thematic Mapper bands 1, 3, 4, and 5 are used as reference images, and one of these, band 5, is presented in Fig. 4. A simulated TM band 7 at 120 m resolution (Fig. 5) was generated by blurring with a 4×4 averaging window and then subsampling. The reference bands were also preblurred and subsampled, followed by application of the LS and frequency replacement method. Using the set of interpolated coefficients on the full resolution reference bands produced the restored TM band 7 in Fig. 6. A comparison of the mean square error (original versus blurred) before enhancement [Fig. 7(a)] and the error (original versus restored) after enhancement [Fig. 7(b)] shows the reduction of error, especially along object borders. In practice, the LS procedure, alone, produces an estimate whose spectrum closely approximates the original data so that the Fourier replacement step may not be necessary.

A second experiment was performed using only the simplified method of frequency replacement. First, the distribution of gray levels for band 5 was normalized to band 7 (using mean and variance). Next, the high spatial frequencies of band 5 were substituted in the degraded band 7. This seemingly good result is shown in Fig. 8. Upon close examination, however, the mean square error is much greater than for the LS approach, as is illustrated in Fig. 7(c) and Table III. The lesser performance of the simple approach is expected since not all edges will be augmented by the correct amount of high frequency correction. The more correlated the reference band is, the better the enhancement will be.

The LS procedure was also applied to TM thermal IR (band 6) data. The original thermal data are presented in Fig. 9. Note the similarity of the overall blurring with the simulated degradation of Fig. 5. Bands 1, 3, 4, 5, and 7 were used as reference bands and were preblurred before applying the LS technique. The LS procedure was applied to produce the enhanced image in Fig. 10.

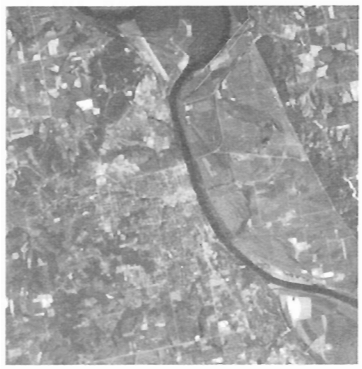

Fig. 3. Original TM band 7 image.

Fig. 4. TM band 5 image used as a reference (30 m resolution).

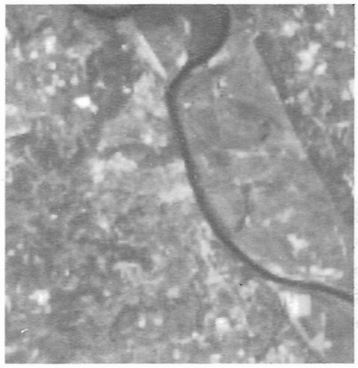

Fig. 5. Band 7 image at 120 m resolution.

Fig. 6. Band 7 image LS-restored.

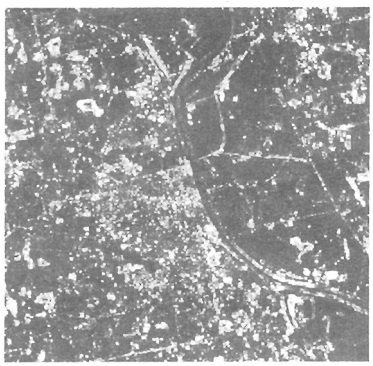

(a)

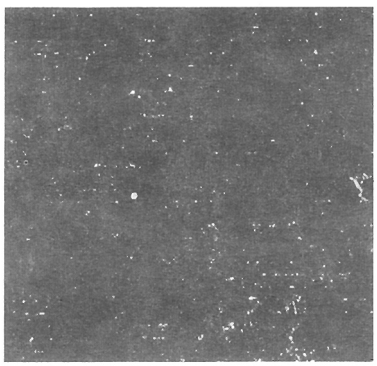

(b)

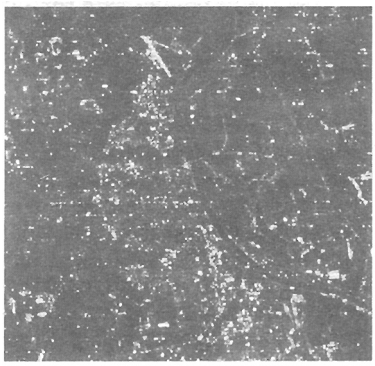

(c)

Fig. 7. Band 7 mean square error: (a) original vs blurred, (b) original vs LS-restored, and (c) original vs filtered with band 5.

Fig. 8. Band 7 restored using band 5 high-pass filtered.

Fig. 9. Original thermal image at 120 m resolution.

Fig. 10. Thermal image LS-restored.

7. SUMMARY

An adaptive multiband image enhancement procedure for improving the apparent resolution of TM thermal band imagery has been described. The adaptive LS technique has been shown to be very effective at exploiting the correlation properties of multiband data in order to perform linear prediction across bands. A simple frequency replacement step that constrains the enhanced data to be consistent with the given data was also described. The effectiveness of the technique was demonstrated by improving the apparent ground resolution from 120 to 30 m for simulated IR and thermal IR imagery.

The adaptive multiband LS approach has other potential applications as well as image sharpening. The basic approach can also be used to estimate radar reflectance from Seasat synthetic aperture radar data using TM images as reference data.[7]

8. REFERENCES

1. R. W. Gerchberg, Opt. Acta 21(9), 709 (1974).
2. R. C. Wrigley, D. H. Card, C. A. Hlavka, J. R. Hall, F. C. Mertz, C. Archwamety, and R. A. Schowengerdt, IEEE Trans. Geoscience and Remote Sens. GE-22 (3), 263 (1984).
3. S. D. DeGloria, IEEE Trans. Geoscience and Remote Sens. GE-22 (3), 303 (1984).
4. P. E. Anuta, IEEE Trans. Geoscience Electronics GE-8 (4), 353 (1970).
5. R. Bernstein, J. B. Lotspiech, H. J. Myers, H. G. Kolsky, and R. D. Lees, IEEE Trans. Geoscience and Remote Sens. GE-22 (3), 192 (1984).
6. T. F. Quatieri, MIT Lincoln Laboratory Technical Report No. 632, Cambridge, Mass. (1983).
7. V. T. Tom and M. J. Carlotto, in *Proc. 1984 Digital Signal Processing Workshop,* IEEE ASSP, p. 1.3.1. (1984).